Mapping the Enantiomerization Routes of Triarylvinyl Propellers. Barriers for the Three-Ring Flip and the Three Different Two-Ring Flips of *m*-Methoxy-Substituted Trimesitylvinyl Isopropyl Ethers[1]

Elimelech Rochlin and Zvi Rappoport*

Department of Organic Chemistry, The Hebrew University, Jerusalem 91904, Israel

Received April 4, 1994[⊗]

E- and *Z*-(*m*-methoxymesityl)-1,2-dimesitylethenols (**3a** and **4a**), their isopropyl ethers **3c** and **4c**, and 1-(*m*-methoxymesityl)-2,2-dimesitylvinyl isopropyl ether (**2c**) were prepared. X-ray structures of **3a** and **3c** were determined. The rotational barriers for the 3-ring flips are 18.8 (**3a**) and 18.3 (**4a**) kcal mol^{-1}. Each of **2c–4c** display two MeO singlets and four *i*-Pr doublets and exist as a mixture of two pairs of enantiomers differing in helicity and in the "up" and "down" disposition of the OMe in relation to the C=C bond. The threshold process for correlated rotation around the Ar–C bonds of **2c–4c** is a three-ring flip which leads to diastereomerization with helicity reversal, with barriers of 15.8–16.1 kcal mol^{-1} resembling that for the three-ring flip enantiomerization of trimesitylvinyl isopropyl ether. The DNMR at the *i*-Pr region showed two coalescence processes. The lower barrier is for a three-ring flip diastereomerization, and the higher barrier is for the two-ring flip enantiomerization of the residual isomers where the MeO-labeled ring passes via the C=C plane. The barriers for the β,β'-, α,β-, and α,β' two-ring flips are 25.2 (**2c**), 23.1 (**4c**), and 21.1 (**3c**) kcal mol^{-1}. MM calculations on the ground-state conformation are in reasonable agreement with the X-ray data, but in the calculated transition states the rings are distorted and the barriers differ from the observed ones. When ring planarity and *o*-Me group constraints are imposed, an agreement of the calculated and observed barriers is achieved. The conformation of the *i*-Pr group significantly affects the calculated barrier. The order of the barriers for the isomeric two-ring flip processes is ascribed mainly to different steric interactions between neighboring rings in the isomeric transition states.

Triarylvinyl systems exist in the solid state[2] and in solution[3,4] in a chiral propeller conformation. In a propeller enantiomerization by a correlated rotation all the rings change in concert the Ar–C=C torsional angles in one enantiomer to the angles in the other enantiomer by both a flip or a non-flip movement.[5] In a flip process the flipping ring passes during the rotation via a plane perpendicular to the double bond plane while concurrently nonflipping rings pass via the C=C plane.[3]

For rings with C_2 symmetry, the possible permutations of conrotatory and disrotatory correlated rotations of the three rings are a one zero-ring flip, three isomeric one-ring flips, three isomeric two-ring flips, and one three-ring flip (the latter four routes are shown in Figure 1). The structures and energies of the transition states for these rotations are different. For understanding the rotational behavior, as many of these barriers as possible should be measured.

There are several obstacles for obtaining several of the barriers. Barriers of 23 ± 2 kcal mol^{-1} are necessary for convenient resolution of such enantiomers for following the enantiomerization by polarimetry. However, most of the barriers are lower than these values. In DNMR, when all the diastereotopic signals coalesce, in the lowest energy enantiomerization process (threshold mechanism), higher energy processes cannot be followed. Moreover, a flip of ring with C_2 symmetry can be followed by DNMR, since it interconverts diastereotopic ortho (or meta) groups with different chemical shifts. However, when such a ring passes during the rotation via the C=C plane a proton is converted to its enantiotopic proton (cf. Figure 7 in ref 3a) and DNMR does not detect changes occurring in this ring. Such changes can be sometimes deduced from changes in the other rings,[3b,c,6] but their observation is frequently difficult.[7]

The last obstacle can be removed by breaking the symmetry of the ring by a meta-substituent since the flip and nonflip rotation of this ring become distinguishable. Looking from a direction perpendicular to the C=C plane, a flip of a ring does not interchange edges, whereas passage through the C=C plane interchanges them. An

[⊗] Abstract published in *Advance ACS Abstracts*, June 1, 1994.

(1) Presented in part in the 52nd Meeting of the Israel Chemical Society, Ramat-Gan, Israel, February 17–18, 1993, Abstr. p 41, and in the 8th European Symposium on Organic Chemistry (ESOC 8), Sitges, Spain, Aug 29–Sept 3, 1993; Abstr. OCB-4.

(2) (a) Kaftory, M.; Biali, S. E.; Rappoport, Z. *J. Am. Chem. Soc.* **1985**, *107*, 1701. (b) Kaftory, M.; Nugiel, D. A.; Biali, S. E.; Rappoport, Z. *Ibid.* **1989**, *111*, 8181.

(3) (a) Biali, S. E.; Rappoport, Z. *J. Am. Chem. Soc.* **1984**, *106*, 477. (b) Biali, S. E.; Rappoport, Z. *J. Org. Chem.* **1986**, *51*, 2245. (c) Biali, S. E.; Nugiel, D. A.; Rappoport, Z. *J. Am. Chem. Soc.* **1989**, *111*, 846.

(4) (a) Biali, S. E.; Rappoport, Z.; Mannschreck, A.; Pustet, N. *Angew. Chem., Int. Ed.* **1989**, *28*, 199. (b) Mannschreck, A.; Rochlin, E.; Rappoport, Z. Unpublished results.

(5) (a) Kurland, R. J.; Schuster, I. I.; Colter, A. K. *J. Am. Chem. Soc.* **1965**, *87*, 2276. (b) Mislow, K. *Acc. Chem. Res.* **1976**, *9*, 26. (c) Mislow, K.; Gust, D.; Finocchiaro, P.; Boettcher, R. J. *Topics in Current Chemistry, No. 47 Stereochemistry 1*; Springer-Verlag: Berlin, 1974; p 1. (d) Willem, R.; Gielen, M.; Hoogzand, C.; Pepermans, H. in *Advances in Dynamic Stereochemistry*; Gielen, M., Ed.; Freund: London, 1985; p 267. (e) Glaser, R. *Alicyclic Organonitrogen Stereodynamics*; Lambert, J. B., Takeuchi, Y., Eds.; VCH: New York, 1992; p 123.

(6) Finocchiaro, P.; Gust, D.; Mislow, K. *J. Am. Chem. Soc.* **1974**, *96*, 2175, had measured several rotational barriers for a single triarylmethyl system.

(7) E.g., for **2c–4c** the A,Ā,B,B̄ mixture (Figure 2) should display at slow exchange 18 Me and 10 ArH singlets, at fast three-ring flip process 9 Me and 5 ArH singlets, and at fast α,β'-two-ring flip enantiomerization 7 Me and 3 ArH signals. Barriers could be therefore measured but due to signal overlap and simultaneous growth, broadening, and coalescence, measurement of the second barrier is mostly impractical.

0022-3263/94/1959-3857$04.50/0

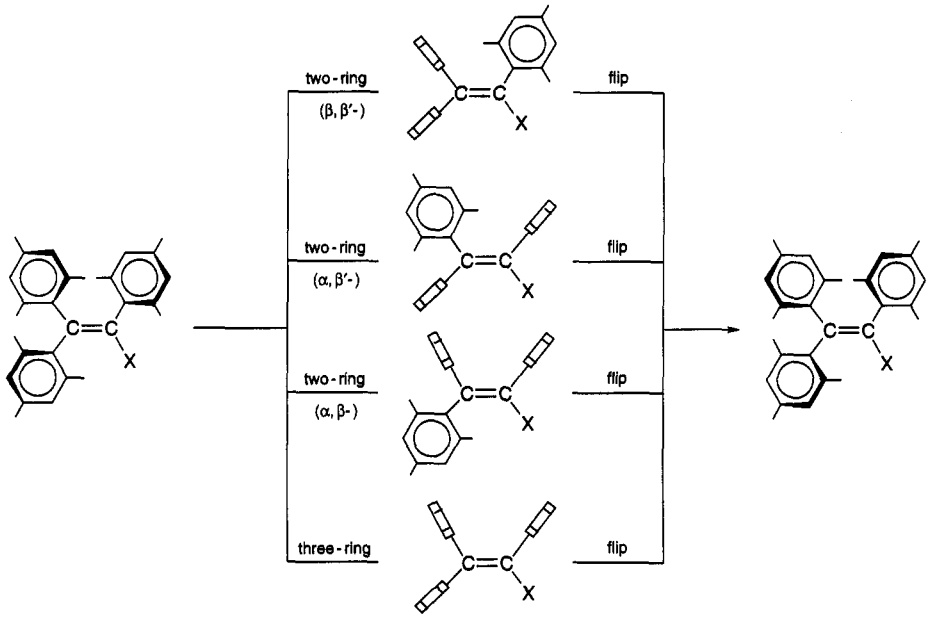

Figure 1. A scheme of the three isomeric two-ring flips and the three-ring flip for a triarylvinyl propeller.

"up" substituent remains "up" after the flip but it is in a "down" position after the ring passes through the C=C plane. Consequently, the system has four stereoisomers which consist of two pairs of enantiomers A,Ā and B,B̄. A three-ring flip no more leads to enantiomerization since the enantiomer of a right-handed propeller with an "up" meta-substituent (e.g. A) is a left-handed propeller with a "down" substituent (i.e. Ā). It leads to diastereomerization (D) (A ⇌ B both with "up" substituent but with opposite helicities). Passage of the meta-substituted ring through the C=C plane is necessary for enantiomerization, which can proceed by two routes E_1 and E_2 (Figure 2). If different DNMR probes are available for enantiomerization and diastereomerization, both can be followed.

We previously found that the threshold rotational process for both trimesitylethenol (**1a**) and its acetate **1b** is a three-ring flip, with barriers of 18.4 and 19.0 kcal mol^{-1}, respectively, measured by coalescence of the *o*-Me or the *m*-H signals.[3a] The diastereomerization of α-*m*-MeO-mesityl acetate **2b** via a three-ring flip gave $\Delta G_c^{\ddagger}$ of 19.0 kcal mol^{-1} measured by MeO coalescence.[4a] Resolution on an optically active column gave the two enantiomers of **2b** and the barrier for their two-ring flip interconversion, where the α-ring passes via the C=C plane was 22.2 kcal mol^{-1} by polarimetry.[4a] A similar study of acetates **3b** and **4b** will be reported elsewhere.[4b]

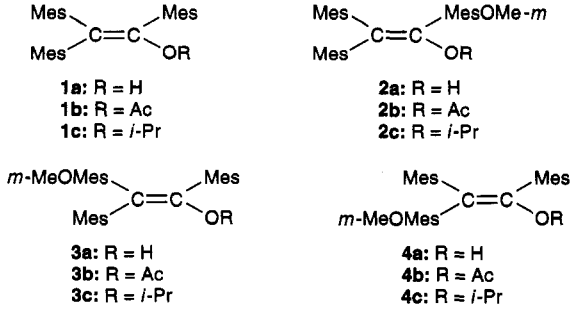

In the present work we use only a DNMR technique. By labeling, in turn, each mesityl ring by a *m*-MeO group, the three isomeric enols **2a**–**4a** and their isopropyl ethers

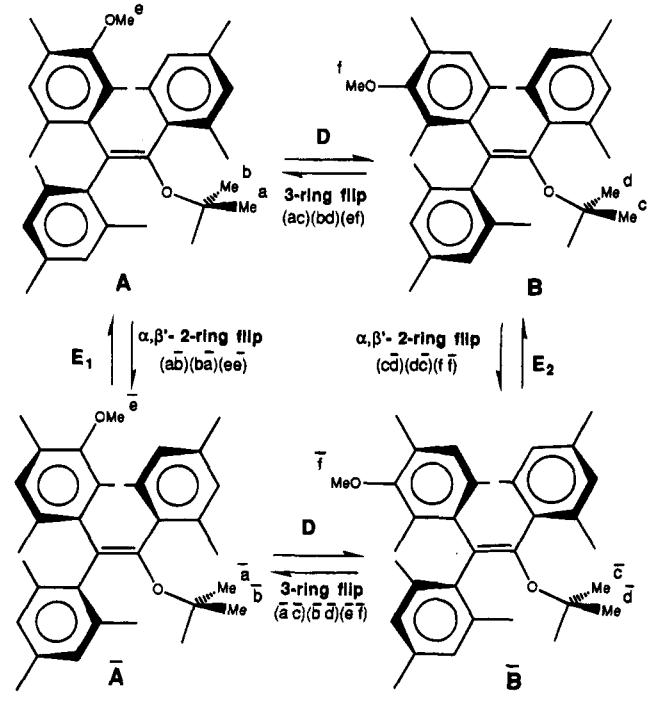

Figure 2. Four stereoisomers of (*E*)-1,2-dimesityl-2-(*m*-methoxymesityl)vinyl isopropyl ether (**3c**) and diastereomerization D (three-ring flip) and two enantiomerization E_1 and E_2 (α,β'-two-ring flip) routes. A and Ā, and B and B̄ are enantiomers; A(Ā) and B(B̄) are diastereomers. a,ā; b,b̄; c,c̄; d,d̄; e,ē; f,f̄ are pairs of diastereotopic protons where letters with bars are enantiotopic sites of letters without bars.

2c–**4c** and that of **1a** (i.e., **1c**) were prepared. A prochiral *i*-Pr group attached to a helical (methoxymesityl) dimesitylvinyl group displays different signals for each of the four stereoisomers A, Ā, B, B̄ (Figure 2). In a three-ring flip diastereomerization two pairs of signals coalesce, and enantiomerization of the "residual enantiomers"[8a] results in coalescence of the two *i*-Pr signals formed in the first coalescence. Hence, the *i*-Pr is both a diastereomerization (as is the MeO) and an enantiomerization probe. This enables us to study the four rotational processes shown in Figure 1, for **2c**–**4c**.

Results

Synthesis. The known[4a] 1-(*m*-methoxymesityl)-2,2-dimesitylethenol (**2a**) was prepared from dimesitylketene and (*m*-methoxymesityl)magnesium bromide. It reacted without further purification with *i*-PrBr under phase-transfer conditions in the presence of $Et_3N^+CH_2PhBr^-$ (TEBA) to give 70% yield (based on the substituted benzene) of **2c** (eq 1).

$$Mes_2C{=}C{=}O + m\text{-MeOMesMgBr} \rightarrow \mathbf{2a} \xrightarrow[\text{TEBA}]{\text{NaOH/}i\text{-PrBr}} \mathbf{2c} \quad (1)$$

A mixture of (*E*)- and (*Z*)-2-(*m*-methoxymesityl)-1,2-dimesitylethenols (**3a** and **4a**) was prepared by reaction of mesitylmagnesium bromide with (*m*-methoxymesityl)-mesitylketene (**6**). The ketene was prepared from acid **5** (obtained from mesitylglycolic acid with methoxymesitylene in $AcOH/H_2SO_4$) with thionyl chloride in pyridine (eq 2). The *E*-enol **3a** crystallized slowly

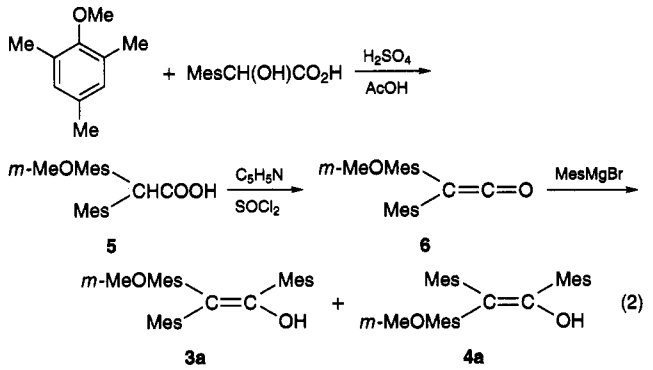

(petroleum ether or MeOH) from the **3a/4a** mixture and assigned by X-ray crystallography which also shows its propeller conformation.[8b] Its ORTEP drawing and important bond lengths, bond angles, and Ar—C=C dihedral angles resembling those of **1a**[2a] are given in Table 1.

A relatively rapid **3a** ⇌ **4a** isomerization takes place in benzene, DMSO, $CDCl_3$, THF, or CCl_4 or on a silica column.[9] Consequently, separation of pure **4a** by crystallization or chromatography was unsuccessful.

Reaction of the **3a/4a** mixture with *i*-PrBr under phase-transfer conditions gave the two isomeric isopropyl ethers **3c** and **4c** in ca. 1:1 ratio (eq 3). They were stable to

$$\mathbf{3a/4a} \xrightarrow[\text{TEBA}]{i\text{-PrBr/NaOH}} \mathbf{3c} + \mathbf{4c} \quad (3)$$

mutual isomerization under conditions when the enols isomerized and were easily separated by chromatography. Initial configuration assignments were based on the near correspondence between the δ(MeO) signals in the enols (of known configuration) and the ethers. For **3a** δ(MeO) = 3.52 (minor stereoisomer), 3.29 (major stereoisomer), and for **4a** δ(MeO) = 3.75 (major stereoisomer), 3.59 (minor stereoisomer). For one isorpopyl ether δ(MeO) = 3.50 (minor stereoisomer), 3.26 (major stereoisomer), and for the other δ(MeO) = 3.76 (major stereoisomer), 3.54 (minor stereoisomer) ppm, suggesting that the ethers are **3c** and **4c**, respectively.

The *E*-structure of **3c** was corroborated unequivocally by X-ray diffraction.[8b] The ORTEP drawing showing the propeller structure, and selected bond lengths and angles, are given in Table 1. The Ar—C=C dihedral angles are 58.7° (α-Ar), 57.6° (β-Ar), and 62.1° (β′-Ar).

The more stable *E*-diastereomer displays the lower δ(OMe)value (3.26), whereas the more stable *Z*-diastereomer has a higher δ(OMe) value (3.76) in line with the X-ray structure and MM calculations (see below) which show that in the most stable structure of both isomers the OMe faces the cis vicinal group. In the *E*-isomer it is Mes, and the MeO is at the shielding zone of the α-ring, while in the *Z*-isomer it is OPr-i, without such a shielding effect.

The R_f values of the *E*-isomers exceed those of the *Z*-isomers. This is probably due to higher dipole moment of the latter, having two reinforcing dipoles on the same side of the double bond.

X-ray Structures of 3a and 3c. Bond lengths and angles for **3a** and **3c** (Table 1) are similar except for a relatively higher O1C1C3 bond angle for **3c**, which is much smaller than the sp^2 angle. The C1—C2 bond lengths of 1.35 Å are slightly longer than the average C=C bond length of 1.34 Å. The C2C1C3 angles of 127–128° are larger than the sp^2 angle of 120°. There are slight, but constant differences, depending on their location, in bond lengths and angles of all rings, e.g. the $C_{ipso}—C_o$ bonds are the longest inter-ring bonds and the $C_m—C_p$ bonds are the shortest. The $C_oC_mC_p$ angles are the widest inter-ring bond angles. Other trends are shown in Table 1.

Static Structures of 2c, 3c, and 4c. All the four stereoisomers predicted for **2**–**4** are observed. For a "frozen" conformation on the NMR time scale, each of **2c**–**4c** should show 4 *i*-Pr doublets and 2 heptets, 2 MeO singlets, and 18 mesityl-Me and 10 mesityl-H singlets in the absence of overlap. The static NMR in $CDCl_3$ at 295 K corroborates the prediction (Table 2). Two *i*-Pr doublets are at δ 0.94 ± 0.01 ppm and two at δ 1.12 ± 0.02 ppm.

At room temperature two sets of signals for the two diastereomers are observed. Integration of the MeO signals gave 1:1 (**2c**), 3:1 (**3c**), and 4:1 (**4c**) ratios. The isopropyl-Me groups show four identical doublets for **2c**, assigned to the different stereoisomers by the DNMR experiment. Of those observed for **3c**, pairs are assigned by their 3:1 ratio. For **4c** the minor stereoisomers consist of only 20% of the mixture and extensive overlap leads to only two broadened doublets. The number of heptets is half of that of the doublets. For **2c** all the expected signals are observed, but 4 pairs of Mes-Me and 2 pairs of Mes-*m*-H overlap. For **3c**, the number of the signals is as predicted except for one overlap in each region, while for **4c** only half of the expected number is observed since signals of the minor stereoisomer are hidden below those for the major one.

Dynamic Stereochemistry. On raising the temperature of samples of **3a**, **4a**, and **2c**–**4c** in $C_6D_5NO_2$ several coalescence processes were observed in the ^1H NMR spectrum. Those for **3a** and **4a** were followed at 200 MHz only in the MeO region, while those for **2c**–**4c** were followed at 400 MHz in the MeO and $CHMe_2$ regions. In

(8) (a) Finocchiaro, P.; Gust, D.; Mislow, K. *J. Am. Chem. Soc.* **1974**, *96*, 3198. See also Iwamura, H.; Mislow, K. *Acc. Chem. Res.* **1988**, *21*, 175 and references therein. (b) The authors have deposited atomic coordinates for this structure with the Cambridge Crystallographic Data Centre. The coordinates can be obtained, on request, from the Director, Cambridge Crystallographic Data Centre, 12 Union Road, Cambridge, CB2 1EZ, UK.

(9) Rochlin, E.; Rappoport, Z. Unpublished results.

Table 1. Observed Bond Lengths and Bond Angles of Solid 3a and 3c, and Calculated (MM2 87) Values for 1c

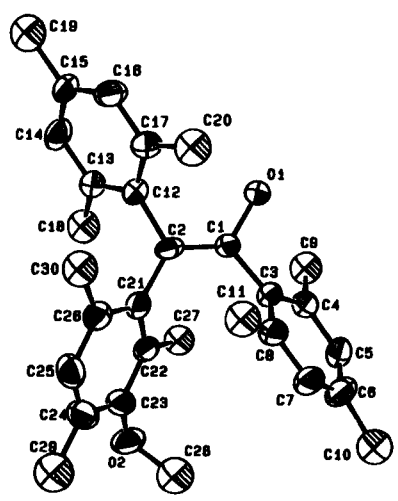

3a

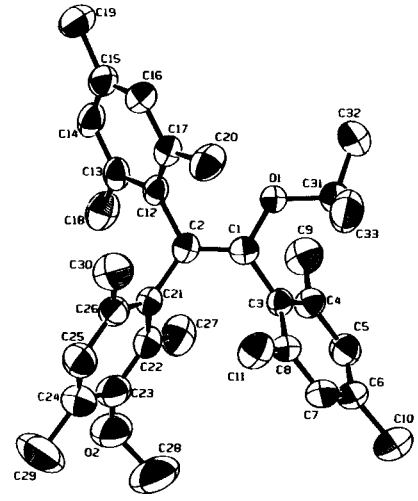

3c

bond	length, Å: 3a[a]	3c[a]	1c[b]	angle	angle, deg: 3a[a]	3c[a]	1c[b]	torsional angle	angle, deg: 3c[a]	1c[b]	dihedral angle	angle, deg: 3a[a]	3c[a]
O1—C1	1.391(6)	1.377(5)	1.372	O1C1C2	122.0(4)	117.1(4)	119.5	O1C1C3C4(α)	57.9	56.8	O1C1C3/α-ring	56.4	58.8
C1—C2	1.352(7)	1.354(6)	1.354	C2C1C3	128.1(5)	127.1(5)	123.2	O1C1C3C8(α)	−120.3	−124.0	C12C2C21/β-ring	51.5	57.6
C1—C3	1.492(7)	1.498(6)	1.485	O1C1C3	109.9(4)	115.3(4)	118.6	C12C2C21C26(β)	57.5	53.3	C12C2C21/β′-ring	57.5	62.1
C2—C12	1.516(7)	1.520(6)	1.518	C1C2C12	119.5(5)	119.9(4)	118.4	C12C2C21C22(β)	−121.7	−126.6	O1C1C3/C12C2C21	6.7	7.1
C2—C21	1.486(7)	1.506(6)	1.516	C1C2C21	121.5(4)	121.7(4)	123.1	C21C2C12C13(β′)	63.6	58.5	O1C1C3/O1C1C31		29.1
O2—C23	1.390(8)	1.394(7)	1.368	C12C2C21	118.9(4)	118.4(4)	118.4	C21C2C12C17(β′)	−119.8	−121.7			
O1—C31		1.457(3)	1.417	C23O2C28	113.9(5)	113.6(5)	114.6	C3C1O1C31(OPr-*i*)	29.2	27.4			
O2—C28	1.44(1)	1.446(8)	1.408	C1O1C31		120.3(4)	121.3	C1O1C31C33(OPr-*i*)	68.4	60.9			
2C31—C_{Me}		1.494 ± 0.004	1.534−1.536	6$C_oC_mC_p$	122.4(6)−124.0(6)	122.3(5)−123.6	121.5−122.4	O1C1C2C12	0.4	−3.0			
6C_{ipso}-C_o	1.402(8)−1.425(8)	1.397−1.416(6)	1.405−1.407		(av 122.8 ± 0.3)	(av 122.9 ± 0.3)		C3C1C2C21	10.3	2.3			
	(av 1.412 ± 0.007)	(av 1.408 ± 0.005)		6$C_{ipso}C_oC_m$	118.2(5)−119.4(5)	118.6(5)−119.8(5)	120.1−120.6						
6C_o-C_m	1.388(8)−1.409(7)	1.393(7)−1.399(8)	1.397−1.398		(av 118.8 ± 0.4)	(av 119.2 ± 0.4)							
	(av 1.399 ± 0.007)	(av 1.395 ± 0.002)		3$C_mC_pC_m$	116.9(6)−117.9(5)	116.8(6)−117.8(5)	117.8−118.1						
6C_m-C_p	1.36(1)−1.391(8)	1.364(8)−1.383(7)	1.391−1.392		(av 117.4 ± 0.3)	(av 117.2 ± 0.4)							
	(av 1.378 ± 0.012)	(av 1.374 ± 0.006)		3$C_oC_{ipso}C_o$	118.7(5)−119.3(5)	117.5(6)−119.7(4)	117.5−118.5						
3C_p-C_{Me}	1.494(1)−1.521(9)	1.513(9)−1.523(8)	1.506−1.507		(av 118.9 ± 0.3)	(av 118.4 ± 0.9)							
	(av 1.506 ± 0.010)	(av 1.517 ± 0.004)		3$C_mC_oC_{Me}$	116.6(6)−118.6(5)	116.2(5)−118.4(5)	114.7−116.7						
6C_o-C_{Me}	1.486(9)−1.510(9)	1.496(8)−1.510(7)	1.508−1.515		(av 117.8 ± 0.6)	(av 117.3 ± 0.6)							
	(av 1.496 ± 0.007)	(av 1.503 ± 0.004)		3$C_{ipso}C_oC_{Me}$	122.3(5)−124.0(5)	122.6(5)−124.5(5)	122.8−124.5						
					(av 123.3 ± 0.6)	(av 123.3 ± 0.6)							
				3$C_mC_pC_{Me}$	118.0(6)−124.1(6)	119.6(7)−123.6(7)	120.1−121.7						
					(av 121.3 ± 1.2)	(av 121.4 ± 0.9)							

[a] Observed. [b] Calculated.

Table 2. ^{1}H NMR (δ values in ppm) of the Dimesityl-(3-methoxymesityl)vinyl Isopropyl Ethers 2c–4c in $CDCl_3$ at 295 K

	Me_2CH		MeAr		MeO		$CHMe_2$		ArH		
isomer	A	B	A	B	A	B	A	B	A	B	A/B
2c	0.93[a]		1.79(2)		3.31		3.82		6.48		1:1
	0.95[a]		1.84		3.73		3.92		6.51		
	1.11[b]		1.88						6.57(2)		
	1.14[b]		1.90(2)						6.64		
			1.91(2)						6.71(×2)		
			2.08						6.84		
			2.12						6.93		
			2.125						6.94		
			2.22								
			2.26(2)								
			2.31								
			2.32								
			2.595								
			2.61								
3c	0.95	0.93	1.81	1.73	3.26	3.50	3.88	3.85	6.57	6.49	3:1
	1.13	1.11	1.83	1.86					6.58	6.59	
			1.86	2.11					6.70	6.68	
			1.88	2.22					6.84	6.82	
			2.10	2.25					6.93	6.93	
			2.19	2.34							
			2.25	2.37							
			2.37	2.61							
			2.59								
4c	0.94		1.73		3.76	3.54	3.84		6.50		4:1
	1.10		1.84						6.57		
			1.86						6.60		
			1.88						6.73		
			2.11						6.83		
			2.23								
			2.25								
			2.34								
			2.55								

[a] Belongs to one diastereomer. [b] Belongs to the other diastereomer.

all cases we used the Gutowski–Holm approximation[10] for the rate constant $k_1 = \pi\Delta\nu/\sqrt{2}$ and the Eyring equation to obtain the $\Delta G_c^{\ddagger}$ values. Since the coalescing signals are mostly of an unequal intensity, the lowest barrier in the direction from the less-abundant to the more-abundant isomer is given.[11] The barrier in the other direction is slightly higher (1 kcal mol^{-1} in the extreme case of **4c**) and is calculated from $k_{-1} = \pi\Delta\nu/K\sqrt{2}$ where K (>1) is the equilibrium constant.[11]

3a and 4a. Due to the rapid **3a** ⇌ **4a** interconversion, coalescence of their MeO signals was studied on their mixture. The signals for **3a** ($\Delta\nu$ = 37.8 Hz) and **4a** ($\Delta\nu$ = 56.6 Hz) coalesce at 376 K and 372 K, respectively, giving $\Delta G_c^{\ddagger}$ values of 18.8 (**3a**) and 18.3 (**4a**) kcal mol^{-1}.

2c. Figure 3 gives the spectrum of **2c** at several temperatures. The number of Ar*H*, *CH*Me_2, OMe, Ar*Me*, and CH*Me*$_2$ signals at 295 K (8, 2, 2, 14, 4) and 450 K (3, 1, 1, 7, 1), respectively (Table 2), is consistent with a slow exchange at 295 K and a fast exchange at 450 K.

The two 1:1 MeO signals ($\Delta\nu$ = 177.4 Hz at 400 MHz at 295 K) coalesce at T_c = 340.5 K, giving a sharp singlet at 390 K (Figure 3a). $\Delta G_c^{\ddagger}$ = 15.9 kcal mol^{-1} for the diastereomerization. For the CH*Me*$_2$ methyls, two regions of four equal signals are observed at 295 K in $CDCl_3$, but in $C_6D_5NO_2$ broadening occurs already at 295 K and in one region only a broad doublet is displayed. Each component of each doublet coalesces with a signal from the other region, $\Delta\nu$ = 50.2 and 38.3 Hz (Figure 3b). A precoalescence broadening of each doublet component leads to two broad signals at 310 K which coalesce at 318.7 K. The derived $\Delta G_c^{\ddagger}$ values are 15.7 and 15.8 kcal mol^{-1}, respectively. At higher temperature first a new doublet and then two equal doublets ($\Delta\nu$ = 2.2 Hz) are formed. (cf. Figure 3b at 425 K). They coalesce to one doublet at 450 K, giving $\Delta G_c^{\ddagger}$ = 25.2 kcal mol^{-1} for this (enantiomerization) process. Since $\Delta\nu$ is low, the error in k_1 is higher than in the other cases and the maximum error estimated is ±0.3 kcal mol^{-1} (Table 3).

3c. Coalescence of the two MeO signals ($\Delta\nu$ = 70 Hz) at 330.7 K (cf. Table 3) give the lowest $\Delta G_c^{\ddagger}$ of 16.1 kcal mol^{-1}. The C*H*Me_2 signals appear in two regions, each showing at 290 K a main doublet for the major stereoisomer and half of a doublet of the minor stereoisomer (the other half is hidden). The minor doublet at one region coalesces with the major one in the other region at 330 K giving two doublets ($\Delta\nu$ = 14.3 Hz), which coalesce at 404 K with $\Delta G_c^{\ddagger}$ = 21.1 kcal mol^{-1} to a single doublet. The number and assignments of signals at 450 K resemble those given for **2c** (Table 3).

4c. Since the minor isomer is only 20% of the mixture, we could not follow the first coalescence in the C*H*Me_2 region. The lower barrier was measured only in the MeO region ($\Delta\nu$ = 254 Hz, T_c = 343 K, $\Delta G_c^{\ddagger}$ = 15.8 kcal mol^{-1}). The second coalescence of the two C*H*Me_2 doublets ($\Delta\nu$ = 9.3 Hz) to one doublet occurred at 434 K, $\Delta G_c^{\ddagger}$ = 23.1 kcal mol^{-1}. The number and assignment of signals at 450 K resemble that for **2c** (Tables 2 and 3).

MM Calculations. For molecular mechanics calculations we used the MM2(87) method (Marcomodel V3.0 program). Previous MM2 calculations of the ground-state structures of tetramesitylethylene[12] and 2,2-dimesityl-1(*R*)-ethenols (R = H, Me)[3c] satisfactorily agree

(10) Gutowsky, S. H.; Holm, C. H. *J. Chem. Phys.* **1956**, *25*, 1228.
(11) Kost, D.; Carlson, E. H.; Raban, M. *Chem. Commun.* **1971**, 656.
(12) Gur, E.; Kaida, Y.; Okamoto, Y.; Biali, S. E.; Rappoport, Z. *J. Org. Chem.* **1992**, *57*, 3689.

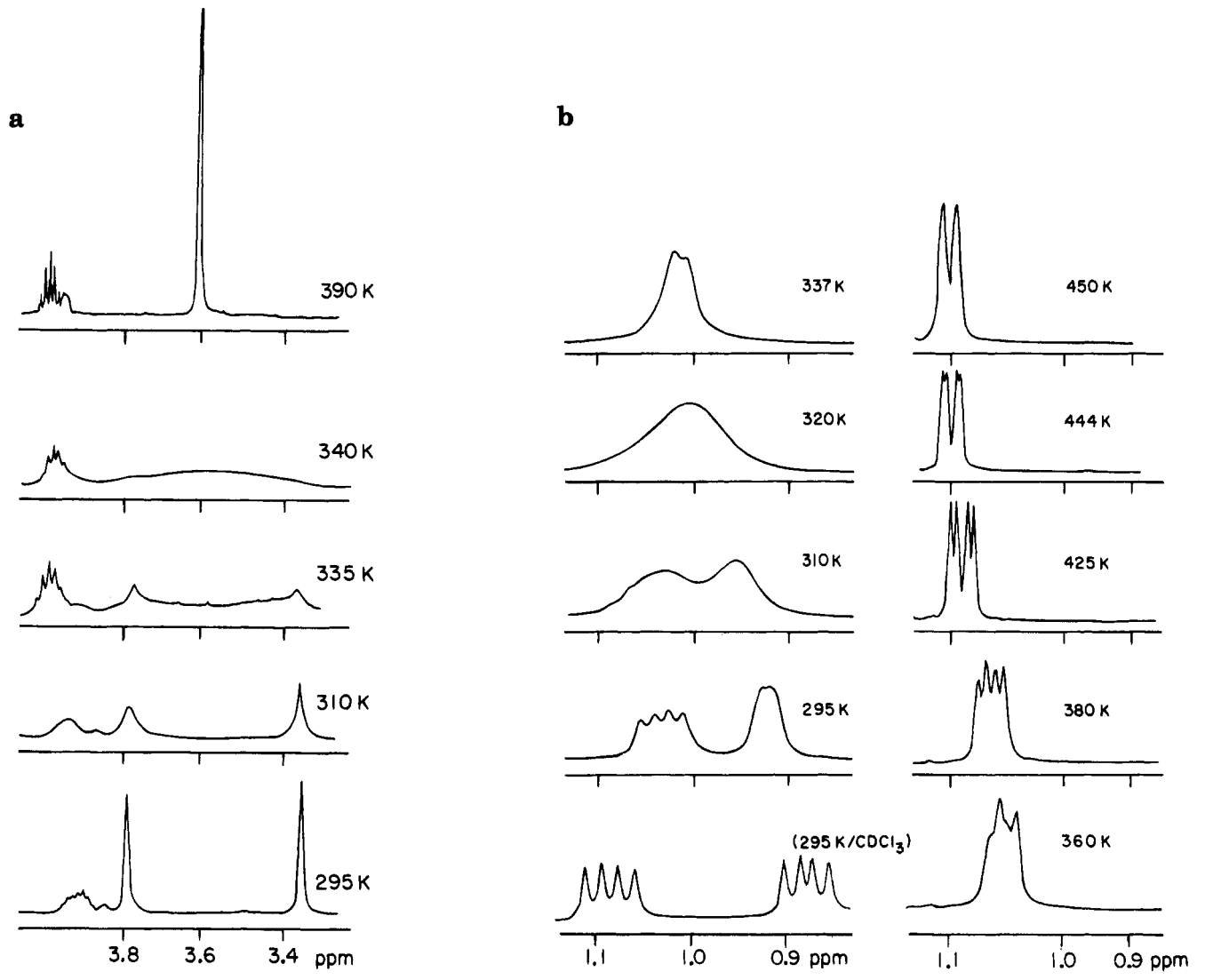

Figure 3. DNMR of **2c**. (a) In the MeO region. Two sharp singlets at 295 K (slow exchange) coalescence at 340 K; a sharp average singlet at 390 K. (b) In the Me_2CHO region. Four doublets are shown at 295 K in $CDCl_3$. The other spectra are at $C_6D_5NO_2$. First coalescence at 320 K; two sharp doublets of the residual isomers are at 425 K. Second coalescence (enantiomerization) is at 450 K.

Table 3. Coalescence Data and Rotational Barriers (in kcal mol^{-1}) for 2c–4c in $C_6D_5NO_2$

compound	diastereomer ratio	coalescing signals	diastereomerization process $\Delta\nu$, Hz	T_c, K	$\Delta G_c^{\ddagger}$	coalescing signals	enantiomerization process $\Delta\nu$, Hz	T_c, K	$\Delta G_c^{\ddagger}$	no. of signals, at $>T_c$[a]
2c	1.02	OMe (ef)(ēf̄)	177.4	340.5	15.9					13[b]
		$CHMe_2$ (ac)(bd) (āc̄)(b̄d̄)	50.2; 38.3	318.7	15.7; 15.8	$CHMe_2$ (ab̄)(bā) (cd̄)(dc̄) (cd̄)(dc̄) (1:1)	2.2	450	25.2	
3c	≈3:1	OMe (ef)(ēf̄)	70	330.7	16.1	$CHMe_2$ (1:1)	14.3	404	21.1	12[c]
4c	4:1	OMe (ef)(ēf̄)	254	343	15.8	$CHMe_2$ (1:1)	9.3	434	23.1	12[d]

[a] In $C_6D_5NO_2$. In each case these include 1 MeO, 1 C*H*Me_2 (h), 1 CH*Me*$_2$ (d), 3 Ar*H* and 6 or 7 Me signals. For the number of signals at $<T_c$ see Table 1. [b] At 450 K. [c] At 437 K. Two Ar*H* and one Me signal are still broad. [d] At 443 K. One Ar*H* is still broad.

with the X-ray data. However, the calculated threshold barriers were lower than the experimental values and the mesityl rings in the calculated transition state structures were significantly distorted.

(a) Ground-State Conformation. The X-ray data for **1a**[2a] and **3a** are very similar,[13] i.e. a *m*-MeO group little affects the ground-state structure. The similarity of the threshold barrier for **2c–4c** and **1c** indicate a small effect on the transition-state energy. Consequently, calculations were first performed on **1c**. Its conformation could be described by the three Ar–C=C angles ϕ_α, ϕ_β,

(13) Most of the bond lengths and angles of **3a** are between the values of the two crystallographically independent molecules of **1a** or similar to one of them. Exceptions are C2–C12 (0.01 Å longer), C2–C21 (0.017 Å shorter), α_4 (1° smaller), ϕ_α (1.4° wider), and the C=C torsion angle (1.3° smaller) (than that of the closer structure of **1a**).

Table 4. Calculated ($\Delta H^{\ddagger}$) (MM2 87) and Observed Barriers ($\Delta G_c^{\ddagger}$) in kcal mol^{-1} for Various Flip Processes of 1c–4c, 9, and 10

				$\Delta H^{\ddagger}$, calcd (constraint)[a]						
				none						
ring flip	compound	$\Delta G_c^{\ddagger}$, obsd	compound	*anti-i*-Pr	*syn-i*-Pr	planar rings	planar rings and *o*-Me	compound	planar ring and *o*-Me	
α,β,β′-three-	**1c**	15.8[c]	**1c**	9.9	14.8	15.3	*b*		A ⇌ B	B ⇌ A
	2c	15.9						**2c**	15.4	14.5
	3c	16.1						**3c**	15.5	14.6
	4c	15.8						**4c**	15.3	15.2
									A ⇌ Ā	B ⇌ B̄
α,β′-two-	**3c**	21.1	**1c**	10.5	18.4	17.1	20.1	**3c**	21.2	23.0
α,β-two-	**4c**	23.1	**1c**	9.5	27.3	20.7	23.9	**4c**	24.7	22.6
β,β-two-	**2c**	25.2	**1c**	22.9	27.3	24.6	29.0	**2c**	24.9[f]	25.4[f]
α,β-two-	**9**[d]	16.8	**9**	8.7		15.4				
α,β′-two-				11.9		19.9				
β,β′-two-				15.5		21.0				
α,β,β′-three-(?)		20.5		12.1		18.3	*b*			
α,α′,β,β′-four-(?)	**10**[e]	39.6	**10**[e]	35.2		40.3	*b*			

[a] Constraints: planar rings = $CC_{ipso}C_oC_m$ = 180°; *o*-Me = $CC_{ipso}C_oC_{Me}$ = 5°; values are for the minima of the energy vs θ_1 curves. [b] Convergence was not achieved in the search for a minimum. [c] Reference 3a. [d] Reference 3b. [e] $\Delta H^{\ddagger}$ = 39.6 kcal mol^{-1}. [f] Only planar ring constraint is used.

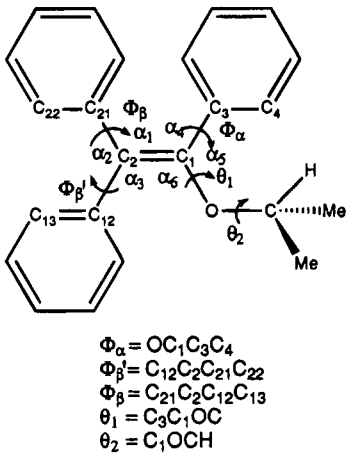

Figure 4. The dihedral angles defining the conformation of a triarylvinyl isopropyl ether, and the bond angles around the double bond.

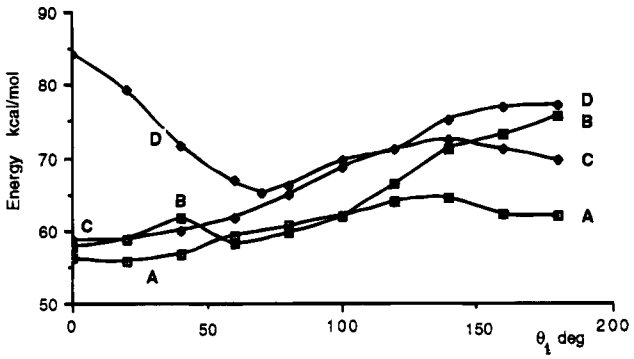

Figure 5. A calculated energy vs angle θ_1 profile for transition states of enantiomerization of **1c**. (A) Three-ring flip; (B) a,β-2-ring flip; (C) α,β′-two-ring flip; (D) β,β′-two-ring flip. The calculated ground-state energy is 40.3 kcal mol^{-1}.

$\phi_{\beta'}$, the $C_{i\text{-}Pr}OC1C_{ipso}$(α-ring) angle θ_1, and the $HC_{i\text{-}Pr}OC1$ angle θ_2 (Figure 4). Different inputs resulted in the same three minima very close in energies (within 0.1–0.2 kcal mol^{-1}), differing mainly in the OPr-*i* conformation. Only one structure displays an antiperiplanar OPr-*i* group (θ_1 = 27°) and resembled the X-ray structure of **3c** (Table 1). The other two displayed an anticlinal arrangement with θ_1 = 61° and unreasonably distorted rings. The barrier calculated for the conformers interconversion is 2 kcal mol^{-1} and only one conformer was observed by NMR in solution.

(b) Transition States. (i) Energies. All five dihedral angles change signs in the enantiomerization, and calculating the full potential energy surface is impractical. Reasonable assumptions concerning the transition-state structures are required in order to get their energies and the simplest one is that they are achiral. These were defined as "ideal"[3a] when the flipping rings are perpendicular to the C=C plane and the nonflipping rings are at the C=C plane, so that both the chirality axis and plane are lost. In addition, in the *i*-Pr conformations, θ_1 and θ_2 values are 0° or 180° (see below).

The conformation of the X group in $Ar_2C{=}C(Ar)OX$ may affect the threshold barrier. In the enols (e.g., **1a**,[3a] **3a**, and **4a**) the OH conformation does not affect the rings rotational barriers since a faster OH rotation than the flip process gives an average C_2 conical symmetry. The barrier for the syn–anti interconversion of the acetate group in **1b**[3a] and in **3b**[9] (12 kcal mol^{-1}) suggest that rotation of the bulky *i*-Pr group cannot be *a priori* neglected. We calculated a barrier for syn–anti interconversion in **1c** of 12 ± 1 kcal mol^{-1}, a value still lower than the three-ring flip barrier.

The transition-state energies were first calculated for the syn and anti conformations, i.e., θ_1 = 180° or 0° when θ_2 = 0°, without other constraints. The barriers for the anti conformation were lower while those for the syn conformation were closer to but still significantly different than the observed barriers (Table 4). The rings, especially the nonflipping ring, were significantly distorted in the transition states. The deviations from planarity, defined as the difference of the torsional $=CC_{ipso}C_oC_m$ angle from 180°, were 17° (α), 28.9° (β), and 25.9° (β′) for the three-ring flip, 1.9° (α), 46.1°(β), and 6.7°(β′) for the α,β′-two-ring flip, and 50.5° (α), 13.1° (β), and 22.2° (β′) for the β,β′-two-ring flip.

We then imposed a constraint of ring planarity enforcing the $=CC_{ipso}C_oC_m$ angles to be 180°. The *i*-Pr conformation was changed gradually by 20° from anti (θ_1 = 0°) to syn (θ_1 = 180°), starting with θ_2 = 0° (i.e., the *i*-Pr methyls are away from the *o*-Me group on the α- and β′-rings; when θ_1 = 0° or 180°, the transition state is achiral), giving energy vs θ_1 profiles (Figure 5). Only for the transition state of the β,β′-two-ring flip θ_2 was changed without limitation; otherwise the calculated minimum much exceeds the experimental value.

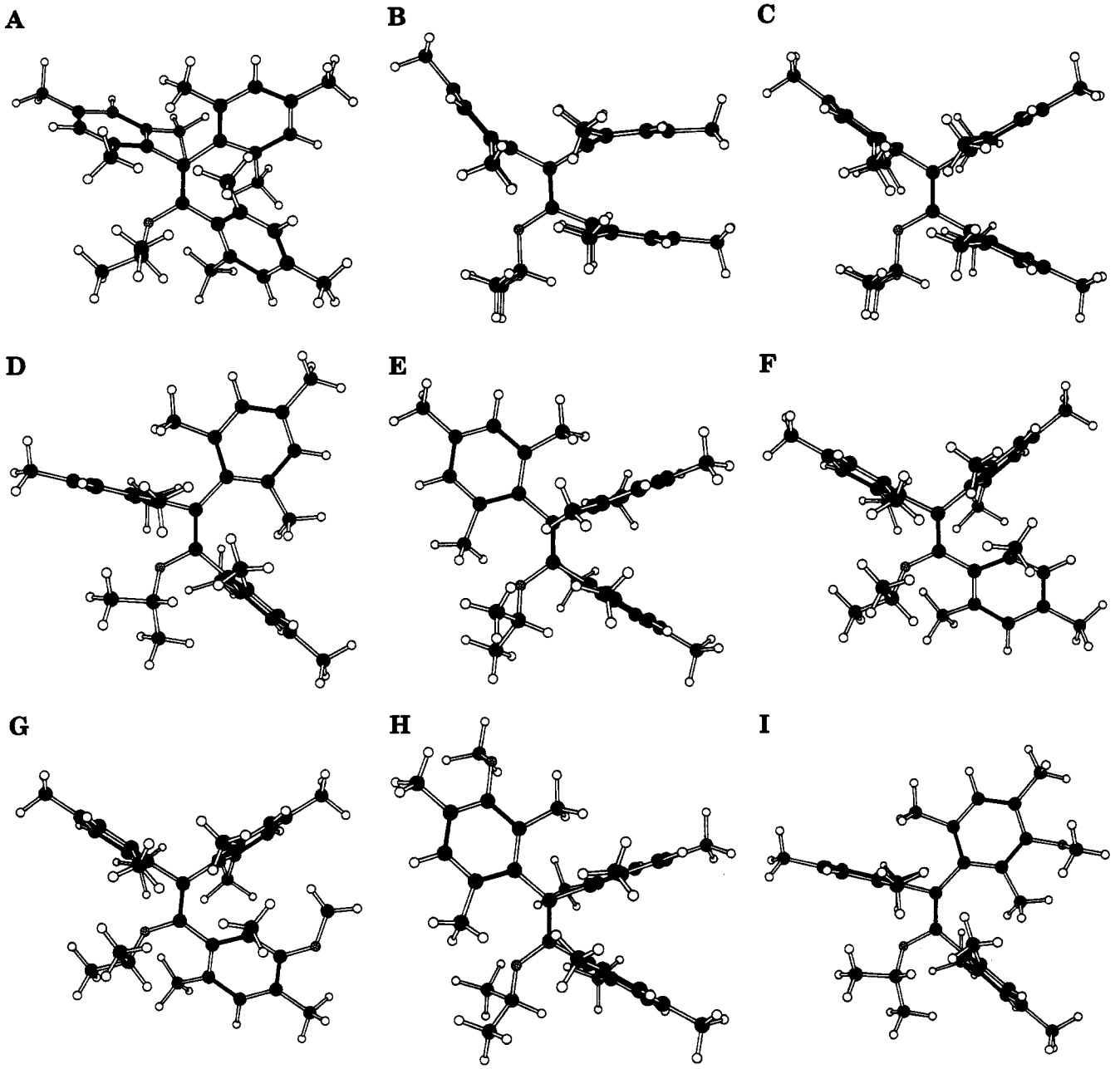

Figure 6. Calculated (MM2) ground-state and transition-state structures for four flip processes of **1c**. (A) ground state; (B) transition state for the three-ring flip without constraints; (C) as in B, plus ring planarity constraints; (D) transition state for the α,β'-two-ring flip with ring planarity and *o*-Me planarity of the nonflipping ring constraints; (E) transition state for the α,β-two-ring flip with ring planarity plus *o*-Me planarity of the nonflipping ring constraints; (F) transition state for the β,β'-two-ring flip with ring planarity constraint; (G) the most stable transition state (E_1) for the α,β'-two-ring flip of **3c**; (H) the most stable transition state (E_2) for the α,β-two-ring flip of **4c**; (I) the most stable transition state (E_1) for the β,β'-two-ring flip of **2c**.

Figure 5 reveals a few important features. (a) In line with experiment, line A for the three-ring flip is the lowest, and line D for the β,β'-two-ring flip is the highest. (b) Line C for the α,β'-two-ring flip is mostly above line B for the α,β-two-ring flip, except around 40° and 150–180° when the order is reversed. (c) The minima for the three-ring and α,β'-two-ring flips plots are around $\theta_1 = 0°$, in line with an achiral transition state. The profile for the α,β-two-ring flip displays two minima, at 0° and at 60°, indicating the possibility of both achiral and chiral transition states. The minimum at ca. 75° in the β,β'-two-ring flip plot is consistent with a chiral transition state. (d) The calculated barriers are 15.2 kcal mol^{-1} at $\theta_1 = 0$ for the three-ring flip, and 24.6 kcal mol^{-1} for the β,β'-2-ring flip at the minimum, compared with the observed 15.8 and 25.2 kcal mol^{-1}. For the α,β- and the α,β'-two-ring flips agreement between calculated (ca. 16.1 and 17.1 kcal mol^{-1}) and observed (23.1 and 21.1 kcal mol^{-1}) barriers is less satisfactory. (e) Only around the local maximum at ca. 40° the calculated barrier of 20.7 kcal mol^{-1} for the α,β-two-ring flip (Table 4) exceeds that for the α,β'-two-ring flip, but it is still 2.4 kcal mol^{-1} lower than the experimental value.

The calculated structures of the two-ring flip transition states (Figure 6) show a severe distortion of the *o*-Me groups from the plane of the nonflipping ring. The *o*-Me facing the vicinal *cis*-ring is always more distorted than that facing the geminal ring. The largest distortions (49.1°; 22.4°) are for the α-ring *o*-Me groups in the β,β'-two-ring flip. These distortions were arbitrarily "cor-

Table 5. Selected Bond Lengths and Angles for the Calculated Transition States and Differences from the Corresponding Ground-State Parameters (Δ) for Several Enantiomerization Processes of 1c

process	bond	length, Å	(Δ, Å)	nonbonded distance, Å		(Δ, Å)	angle	angle, deg	(Δ, deg)	torsional angle	angle, deg
α,β,β′-three-ring flip	C1–C2	1.353	(0?)	O1–C3	2.509	(+0.068)	O1C1C3	122.9	(+4.3)	C3C1O1C31	0
	C1–O1	1.369	(−0.003)	O1–C12	2.806	(+0.079)	C2C1C3	118.3	(−4.9)	C1O1C31H	0
	C1–C3	1.487	(+0.002)	C3–C21	2.837	(−0.14)	C1C2C21	120.8	(−2.3)	O1C1C2C12	<1[b]
	C2–C12	1.522	(+0.004)	C12–C21	2.609	(−0.009)	C12C2C21	117.6	(−0.8)	C3C1C2C21	<1[b]
	C2–C21	1.524	(+0.008)	C9–C27	3.491	(−0.341)	C1C2C12	121.4	(+4.3)		
				C18–C27	3.250	(−0.226)	O1C1C2	118.8	(−0.7)		
				C9–C18	4.155	(−0.722)					
				C9–C32	3.754	(−0.225)					
				C18–C32	4.292	(−0.365)					
α,β′-two-ring flip	C1–C2	1.360	(+0.006)	O1–C3	2.362	(−0.087)	O1C1C3	111.6	(−7.0)	C3C1O1C31	36.8
	C1–O1	1.381	(+0.009)	O1–C12	3.368	(−0.359)	C2C1C3	131.1	(+7.9)	C1O1C31H	31.2
	C1–C3	1.474	(−0.011)	C3–C21	3.460	(+0.483)	C1C2C21	137.0	(+13.9)	O1C1C2C12	2.7[b]
	C2–C12	1.516	(+0.031)	C12–C21	2.641	(+0.023)	C12C2C21	119.2	(+0.8)	C3C1C2C21	2.0[b]
	C2–C21	1.547	(+0.002)	C3–C27	2.887	(−0.523)	C1C2C12	103.8	(−14.6)		
				C12–C30	2.767	(−0.243)	O1C1C2	117.3	(−2.2)		
α,β-two-ring flip	C1–C2	1.365	(+0.011)	O1–C3	2.381	(−0.061)	O1C1C3	112.9	(+5.7)	C3C1O1C31	44.0
	C1–O1	1.362	(−0.01)	O1–C12	3.166	(+0.439)	C2C1C3	121.6	(−1.6)	C1O1C31H	−24.2
	C1–C3	1.493	(+0.008)	C3–C21	2.741	(−0.236)	C1C2C21	111.3	(+11.8)	O1C1C2C12	9.5[b]
	C2–C12	1.550	(+0.032)	C12–C21	2.627	(+0.009)	C12C2C21	118.0	(−0.4)	C3C1C2C21	20.2[b]
	C2–C21	1.515	(−0.001)	C18–O1	1.521	(−0.889)	C1C2C12	130.4	(+12)		
				C20–C21	1.770	(−0.240)	O1C1C2	125.4	(+5.9)		
β,β′-two-ring flip	C1–C2	1.362	(+0.008)	O1–C3	2.460	(+0.018)	O1C1C3	118.0	(−0.6)	C3C1O1C31	79.0[c]
	C1–O1	1.368	(−0.004)	O1–C12	2.646	(−0.081)	C2C1C3	121.7	(−1.5)	C1O1C31H	−57[c]
	C1–C3	1.501	(+0.016)	C3–C21	3.026	(+0.049)	C1C2C21	124.8	(+1.7)	O1C1C2C12	8.7[b]
	C2–C12	1.530	(+0.012)	C12–C21	2.579	(−0.039)	C12C2C21	114.9	(−3.5)	C3C1C2C21	3.4[b]
	C2–C21	1.530	(+0.014)	C9–O1[a]			C1C2C12	117.1	(−1.3)		
				C11–C21[a]			O1C1C2	115.0	(−4.5)		

[a] The *o*-Me groups of the α-ring are highly twisted so that these distances are elongated. [b] The average of the two angles for each process is the torsional angle of the double bond. [c] The pyramidalization of C1 is 27° and of C2 is 21°. In the α,β- and α,β′-two-ring flip processes the pyramidalization at C1 and C2 is ≤5°.

rected" by imposing additional constraint that none of them can exceed 5°. This invariably increases the energy of the two-ring flip transition states. The minima in the energy vs θ_1 profiles for the α,β′- and α,β-two-ring flip transition states shift to $\theta_1 = 30-40°$ giving barriers of 20.1 and 23.9 kcal mol^{-1}, respectively. The barrier for the β,β′-two-ring flip increases to 29 kcal mol^{-1}, well above the experimental value (Table 4).

Three questions were further investigated. (i) To what extent does a *m*-MeO group affect the calculation results for **1c**? (ii) Which is the more-stable diastereomer in **2c–4c**? (iii) Since the *m*-MeO substituent can occupy two sterically different positions, which of the two enantiomerization processes (Figure 2) is preferred? Calculations on **2c–4c** gave the following answers.

For **2c–4c**, the diastereomer where the *m*-MeO group faces the *cis* vicinal group (e.g., **7**) is more stable than diastereomer **8** where it faces the geminal group. For **2c**, ^{1}H NMR shows diastereomers ratio of 1.02–1.05, favoring that with a higher field MeO, which should be an analog of **7** whose OMe faces the β-ring.

In **3c** the MeO hydrogens in A are nearly above the α-ring plane at an average distance of 3.18 Å. Whereas in B (Figure 2), the MeO hydrogens are ≥4.3 Å away from the β′-ring plane. Consequently, the higher field MeO signal of **3c** is of higher intensity than the other signal.

In **4c** the MeO group in **7** faces the OPr-*i* group, whereas in **8** it is mainly influenced by the ring current of the β-ring. Consequently, in the ^{1}H NMR spectrum of **4c** the low-field MeO signal is more intense.

The calculated barriers for the three-ring flip diastereomerization of **2c–4c** in both directions (A ⇌ B, B ⇌ A) are 14.5–15.5 kcal mol^{-1}, resembling that calculated for **1c**. For the two-ring flip enantiomerizations the calculated values differ from those for **1c**, and significant differences exist between the barriers (Table 4) for the

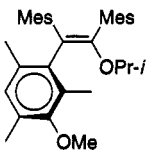

7

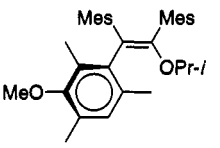

8

two enantiomerization processes E_1(A ⇌ Ā) and E_2(B ⇌ B̄) (Figure 2). The structures of low-energy transition states for **2c–4c** are given in Figure 6G–I. The energy changes accompanying the interconversion of the four stereoisomers are demonstrated in the reaction profile involving rotation of the β′-ring of **4c** (Figure 7). Similar profiles are obtained for rotation of the α- or the β-ring in **2c** and **3c**.

All the transition states were tested by the M test and had a saddle point structure, except for that of the β,β′-two-ring flip. The significant bond lengths, nonbonded distances, and bond and torsional angles of the calculated transition states and differences from the ground state values are given in Table 5.

The "ring planarity" constraints were also applied for two systems which previously showed discrepancies between calculated and observed barriers. The constraints reduced significantly the discrepancy for both trimesitylethylene (**9**)[3b] and tetramesitylethylene (**10**)[12] (Table 4), indicating that the constraints have significant chemical meaning.

9 **10**

(ii) Calculated Structures. Comparison of the calculated structures of the four transition states with the ground state structure of **1c** (Table 5) reveal several trends.

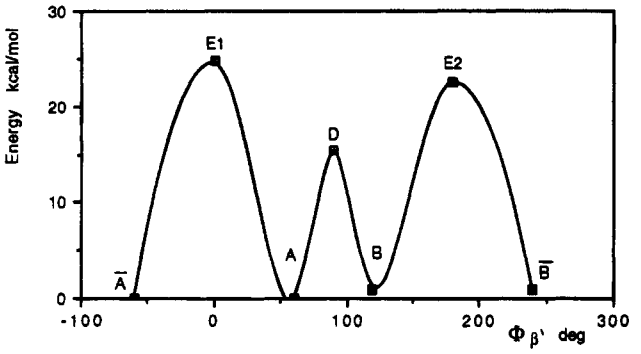

Figure 7. Calculated energy vs ϕ_β plot for rotation of the β'-ring of **4c**. The minima are for the ground state of A,Ā (relative energy 0 kcal mol^{-1}) and B,B̄; the maxima are for the transition states E_1 and E_2 of the α,β-two-ring flip and for the three-ring flip.

Three-Ring Flip. In the transition state the α- and β-rings become closer, the C_{ipso}(α-ring)–C_{ipso}(β-ring) distance being 0.14 Å shorter than in the ground state. Simultaneously, the α- and β′-rings draw apart from the OPr-*i* oxygen and the C_{ipso}–O distances increase by 0.067–0.079 Å. The β-/β′-rings distance remains unchanged. The bond angles α_5 and α_3 widen, while α_4 and α_1 decrease appreciably (Table 5).

The C1–C3, C2–C12 and C2–C21 bonds lengthen by <0.01 Å, the C1–O1 bond length decreases by 0.003 Å, and the C1–C2 bond length does not change. These changes are shown schematically in **11** (Figure 8). The main change is a significant shortening of nonbonded *o*-Me/*o*-Me, *o*-Me/C*H*Me$_2$ distances. Those for geminal or vicinal cis rings or ring/OPr-*i* groups are 0.225–0.365 Å, whereas shortening of the C9–C18 distance for *o*-Me group in trans rings is by 0.722 Å (Table 5).

α,β′-Two-Ring Flip. The calculated transition state shows a significant shortening of the C_{ipso}(β′-ring)–vinylic O distance by 0.359 Å and a lower shortening of the C_{ipso}(α-ring)–O distance. The C_{ipso}(α-ring)–C_{ipso} (β-ring) distance increases strongly while the C_{ipso}(β-ring)–C_{ipso} (β′-ring) distance increases slightly. Changes in the bond angles (e.g., α_3 −14.6°, α_1 +13.9°) are given in Table 5 and are demonstrated in **12** in Figure 8.

The C1–C2 and the C1–O bonds lengthen by <0.01 Å and C2–C12 by 0.031 Å due to steric interaction of the *o*-Me group of the nonflipping β ring with the α and β′ rings. A simultaneous shortening of the C1–C3 distance is presumably due to the increased *o*-Me(α-ring)/*o*-Me(β-ring) distances. The two Me(β-ring)/C_{ipso}(α- or β′-ring) distances of 2.887 and 2.767 Å are smaller than the sum of the Van der Waals radii. The distances between the centers of the rings are α-ring/β-ring 5.51 Å; β-ring/β′-ring 5.07 Å.

α,β′-Two-Ring Flip. The calculated transition state structure indicates a significant shortening (0.236 Å) of the C_{ipso}(α-ring)–C_{ipso} (β-ring) distance and a smaller one for C_{ipso}(α-ring)/OPr-*i* oxygen. Simultaneously, C_{ipso}(β′-ring) is drawn apart from this oxygen by 0.439 Å. The C_{ipso}(β-ring)–C_{ipso}(β′-ring) distance increases slightly. Important changes in bond angles are: α_1 −11.8°; α_3 = 12° (Table 5). These changes are demonstrated in **13** (Figure 8).

The C1–C2 and C2–C12 bonds lengthen significantly, and the C1–O bond length shortens (Table 5), indicating that the *o*-Me groups of the β′-ring are drawn away from both the *i*-Pr methyl and the β(*o*-Me). The *o*-Me(α-ring)/*o*-Me(β-ring) distance of 3.13 Å is shorter than in the transition state of the three-ring flip. Consequently, bond C1–C3 to the α-ring lengthens. The increased *o*-Me(α-ring)/*o*-Me(β-ring) interaction is apparently balanced by decreased interaction with the *o*-Me(β′-ring) groups. Consequently, the C2–C21 bond length changes very little. Entrance of the β′-ring into the C=C plane results in severe repulsions, evident by strong decrease of the *o*-Me(β′-ring) distances from C_{ipso}(β-ring) and O(*i*-PrO) (Table 5). The increased α-ring/β-ring and β′-ring/OPr-*i* repulsions lengthen the C=C bond and increase its torsion angle. The distances between the centers of the rings are α-ring/β-ring 4.1 Å; β-ring/β′-ring 5.08 Å.

β,β′-Two-Ring Flip. Changes in distances between rings and in bond angles in the transition state are milder than those for other two-ring flips, in spite of the larger steric effects reflected by higher energy of this transition state. The increase in the α-ring/β-ring and α-ring/OPr-*i* interactions result in strong distortion of the *o*-Me from the ring's plane. The decreased C_{ipso}(β′)–O(*i*-PrO) distance and the changes in bond angles (Table 5) are demonstrated in **14** (Figure 8). There is also a significant pyramidalization of C1 and C2 of the double bond.

In contrast with the other cases the distance and angle between the β- and β′-rings are significantly reduced by 0.039 Å and 3.5°, respectively. The distances between the centers of the rings are α-ring/β-ring 4.56 Å; β-ring/β′-ring 4.95 Å. Also, both the C=C bond and all the Ar–C= bonds are elongated whereas the C1–O bond length decreases by 0.004 Å.

Discussion

Methoxy Probe. Previous work had shown a relatively small effect of four *m*-Br substituents on the magnitude of the threshold rotational barrier for a one- or a two-ring flip.[14] Hence, a single *m*-MeO group, having smaller electronic effect and effective bulk than *m*-Br should negligibly affect the barriers. Indeed, within experimental error the three-ring flip enantiomerization barrier for **1c**[3a] is identical with the diastereomerization barriers of **2c** and **4c** and is only slightly lower than that for **3c** (Table 2).

Likewise, the barrier for enol **1a** (18.4 ± 0.1 kcal mol^{-1})[3a] is identical with that of **3a** and 0.4 kcal mol^{-1} lower than that for **4a**, and the three-ring-flip barriers for acetates **2a–d** are nearly identical, being 18.8–19.1 kcal mol^{-1}.[4b,9] A *m*-MeO group also affects very little the geometry of **1c** and **3c**, and the calculated MM three-ring-flip and two-ring-flip barriers (see below). Consequently, using the MeO probe enables generalization of the conclusions to other trimesitylvinyl-X systems.

Effect of the Nonaromatic Vinylic Substituent on the Threshold Rotational Mechanism. Data are available on the magnitude of threshold vs nonthreshold rotational barriers in polyarylvinyl propellers. For 2,2-diaryl-1-R-ethenols **15a–d** the threshold mechanism is a one-ring flip, where the ring cis to the OH flips when R = H, and a two-ring flip when R = alkyl, SiR_3.[3a,c,14,15] The one-ring flip is the threshold mechanism for the *i*-Pr ethers **16a** and **16b**, R = H.[3c,14] The $\Delta G^{\ddagger}$ (two-ring flip)

(14) Eventova, I.; Nadler, E. B.; Rochlin, E.; Frey, J.; Rappoport, Z. *J. Am. Chem. Soc.* **1993**, *115*, 1290.

(15) (a) Nadler, E. B.; Rappoport, Z. *Tetrahedron Lett.* **1991**, *32*, 1233. (b) Faragi, E. Z.; Frey, J.; Rappoport, Z. 11th IUPAC Conference on Physical Organic Chemistry, Ithaca College, Ithaca, NY, August 2–7, 1992, Abstr. C–13. (c) Frey, J. Unpublished results.

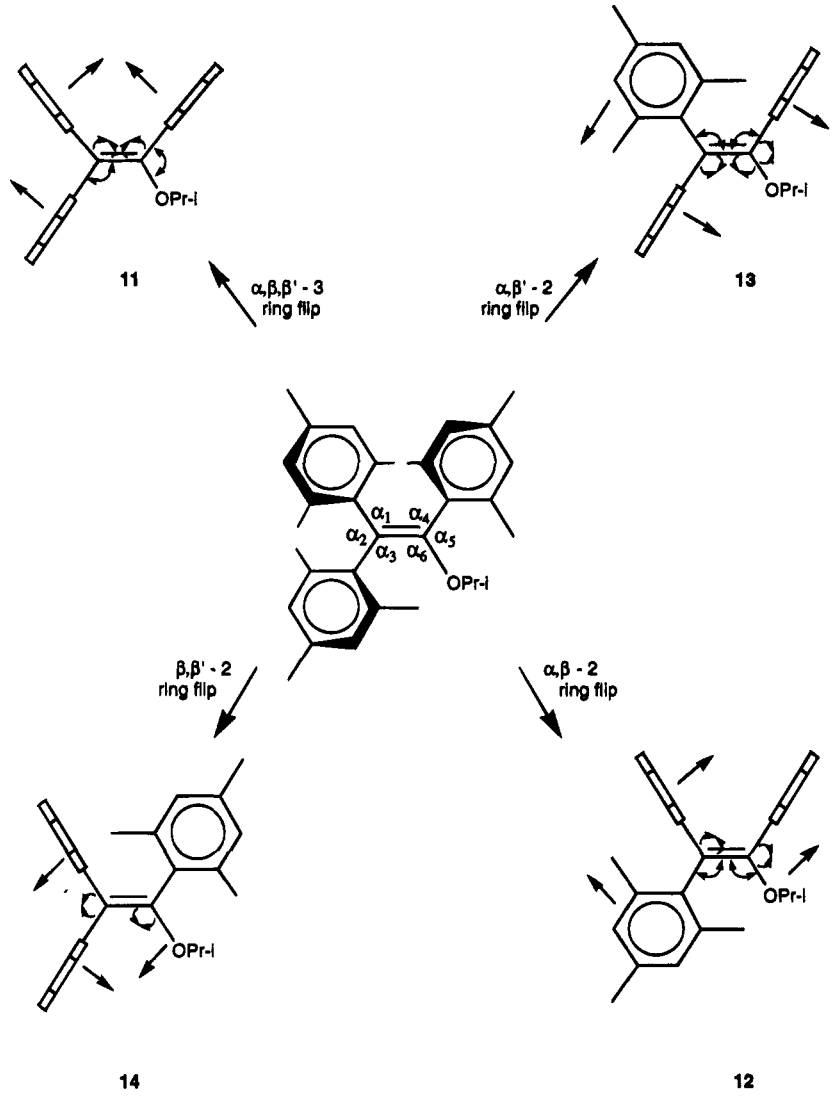

Figure 8. Schematic movements of the rings in the transition states for rotation. (11: In the three-ring flip; **12**: in the α,β-two-ring flip; **13**: in the α,β′-two-ring flip; **14**: in the β,β′-two-ring flip.

$-\Delta G_c$ (one-ring flip) values are 3.8, 0.9, 0.8, 3.0, and 1.0 kcal mol^{-1} for **15a**, **15b**, **15c**, **16a**, and **16b**, R = H,[3a,c,14,15b] respectively. The $\Delta G_c^{\ddagger}$ (*i* Pr ether) $-$ $\Delta G_c^{\ddagger}$ (enol) differences when R = H are 0.7 and -0.1 kcal mol^{-1} in $(CD_3)_2$-CO for the one- and the two-ring flips for **16a/15a**, respectively, and 0.9 and 0.8 kcal mol^{-1} for the **16b/15c** pair in 3:7 CS_2/CD_2Cl_2, respectively.[14] Consequently, the order of the threshold and nonthreshold barriers is *i*-Pr ethers ≥ enols.

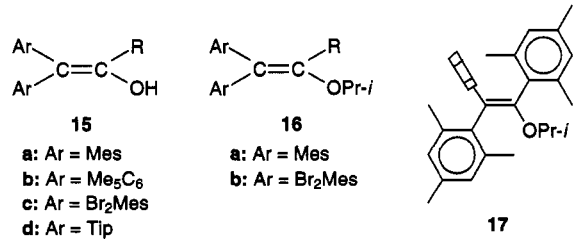

For trimesitylethylene **9**[3b] the threshold barrier is for the α,β-two-ring flip when the ring cis to the H enters the C=C plane in the transition state, and $\Delta G^{\ddagger}$ (three-ring flip) $-$ $\Delta G^{\ddagger}$ (α,β-two-ring flip) ≥ 3.7 kcal mol^{-1}. For acetate **2b** the $\Delta G^{\ddagger}$ (three-ring flip) $-$ $\Delta G^{\ddagger}$ (β,β′-two-ring flip) = -3.2 kcal mol^{-1}.[4a]

Our work extends the rule of a higher energy for the two- compared with the three-ring flip, when the vinylic substituent ≠ H. For the three isomeric two-ring flips, $\Delta G^{\ddagger}$ (three-ring flip) $-$ $\Delta G^{\ddagger}$ (any two-ring flip) = -5 to -9.3 kcal mol^{-1}. Hence, increased number of rings (or bulky substituents) increase the difference in the barriers between *n* and *n* − 1 ring flips.

Barriers for higher energy flip processes were not measured, but that for β-one-ring flip (transition state **17**) for **1c** was calculated as 36 kcal mol^{-1}. The calculated transition state shows a twist of 16° for the C=C bond and pyramidalization of C1 by 36° and of C2 by 34°.

Structural Changes Accompanying the Flip Processes. The calculated transition states diagrams (Table 5, Figure 6) show that except for changes in ϕ_α, ϕ_β, and $\phi_{\beta'}$ the main structural features accompanying the flip processes are as follows.

(a) Three-Ring Flip. *o*-Me groups on different rings become significantly closer in the transition state. For neighboring rings these *o*-Me/*o*-Me distances are smaller than the sum of van der Waals distances. Partial relief of the apparent repulsive interaction is achieved by a small elongation of the =C—Ar bonds.

(b) α,β′- and α,β-Two-Ring Flips. The steric interactions also increase in the transition state where the

o-Me groups of the nonflipping ring "push" strongly neighboring groups in the direction of the group trans to it. The bonds to the two flipping rings are elongated. In the α,β-two-ring flip the α-ring/β-ring distance is significantly shorter than the effective thickness of the rings.

(c) β,β′-Two-Ring Flip. Figure 6 shows that the transition states deformations in cases a and b above are mainly in the spaces between the α- and β-rings and the β′-ring and the *i*-PrO group. The space between the β- and β′-rings is relatively little affected. The rigidity to compression is ascribed to the strong repulsion present between the β- and β′-rings in the ground state, where the C_{ipso}(β-ring)/C_{ipso}(β′-ring) distance is lower than the sum of the van der Waals radii. The reason for the rigidity to widening is unclear. In contrast, in the β,β′-2-ring flip, the β-ring/β′-ring distance is reduced and consequently, increased steric interactions between the rings and the α-ring and its neighbors contribute to the higher energy of this process.

These changes qualitatively resemble those observed for **9** with three main differences. (a) In the transition state for the α,β-two-ring flip of **9** α_3 widened less (6.3°) than in **1c** (12°), due to a weaker H/β′-ring interaction than a OPr-*i*/β′-ring interaction in **1c**. (b) There are larger changes in bond angles of the β,β′-two-ring flip which decrease the transition state crowding more than in **1c**. (c) In contrast with **1c**, unusual distortions of the *o*-Me group of the nonflipping ring are absent.

Conformation of the OPr-*i* Group. The OAc conformation of **1b** is anti in the solid state.[3a] In solution it can be converted to the syn-conformation.[9] An anti ⇌ syn conformational change of the OPr-*i* group was not detected by a DNMR experiment. The MM calculated barrier for it is 11−13 kcal mol^{-1}, but since the syn conformer is 6 kcal mol^{-1} higher in energy than the anti conformer it is not observed by NMR.

Energies of the Isomeric Transition States for Helicity Reversal. If the small effect of the *m*-MeO group is neglected, the present study is a rare example of experimental determination of the energies of four "isomeric" transition states with different geometries for helicity reversal.

The order of these energies is three-ring flip < α,β′-two-ring flip < α,β-two-ring flip < β,β′-two-ring flip. As shown in Table 4 calculations without constraints or even with a "planar rings" constraint do not reproduce the order and magnitudes of the barriers. Only when the two transition states for enantiomerization E_1 and E_2 are considered[16] for **2c**−**4c**, the ring planarity and *o*-Me group planarity constraints lead to good agreement between observed and "lower calculated" transition state barriers except for the β,β′-two-ring flip (Table 4). Since for **9**, **10**, the three-ring flip of **2c**−**4c**, and the β,β′-two-ring flip the *o*-Me constraint is unnecessary, but it reproduces the experimental data in the other cases, caution should be exercised when discussing the calculated barriers and geometries.

Entrance of a ring into the C=C plane in the transition state is mostly energetically more expensive than its flip, and the threshold mechanism mostly involves the largest number of flipping rings. Two main factors contribute to this situation. First, a steric factor, since entrance of an *o*,*o*′-disubstituted ring into the C=C plane results in bumping into geminal or vicinal ring(s) or substituent(s). Only when the small hydrogen is cis to the nonflipping ring is this process the lower energy one, as for **9**[3b] or **15**, R = H.[14,15c] The geometrical changes associated in obtaining the planar Ar—C=C moiety, such as bond angle widening, raise the transition-state energy.

A planar Ar—C=C conjugation also gives a styryl delocalization energy of 4.8 kcal mol^{-1}.[17] About half of this value is already present in the ground state, and the stabilization gained is ca. 2.5 kcal mol^{-1}. Since dipolar hybrids such as **18b** contribute to the structure of vinyl ethers,[18] increased Ar^{β}—C=C or $Ar^{\beta'}$—C=C planarity will decrease the transition state energy by negative charge delocalization (cf. **18c** where $^{-}$Ar indicates a cyclohexadienyl structure with a delocalized charge). However, since the α,β-two-ring flip barrier of 16.8 kcal mol^{-1} for **9** is 6.2 kcal mol^{-1} lower than that for **4c**, this effect is overwhelmed by opposing effects.

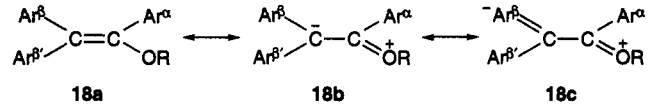

18a **18b** **18c**

A stabilizing T-shape aryl−aryl interaction found in benzene dimer[19] may also slightly lower the transition-state energy for the two-ring flips since the relevant distances of the aryl rings are 4.56−5.51 Å.

Steric and conjugation effects also affect the flip of the rings. The loss of the Ar—C=C conjugations in a flip process raises the transition-state energy. In the three-ring flip transition state it mostly amounts to 7−8 kcal mol^{-1} [17] since the Ar—C=C dihedral angles are >50° in the ground state. The loss is lower in the two-ring flip. All the transition state energies are much higher than this value. Aryl−aryl attractions of "stacked" aryl groups at distances of 4.1 and 4.95 Å, which are also partially present in the ground state, seem to contribute little. Hence, the energies are dominated by steric effects.

These effects reflect repulsion between neighboring groups, opposing the shifts of groups displayed in Figure 8. The consequent changes in bond lengths and angles are documented in Table 5, in Results and in Figure 8. An example is the interaction between C_{ipso} of rings α, β, and β′ and the OPr-*i* group. The ground-state distances between C_{ipso} of geminal and cis-vicinal rings are already lower than the van der Waals distances, and the C_{ipso}-(α-ring)/O and C_{ipso}(β′-ring)/O distances are lower than the sum of O van der Waals radius and half-thickness of the ring.

The multitude of effects suggest that quantitative dissection of the order of the barriers to its components is difficult. A qualitative analysis leads to the following conclusions.

Entrance of a ring into the C=C plane is energetically more costly when it is neighbor to the OPr-*i* group. The highest and the second higher barriers are for a nonflip-

(16) In our work the E_1 and E_2 processes could not be independently followed, in contrast with ref 6, since diastereomerization rather than enantiomerization is the threshold process, so that edges are exchanged before the enantiomerization is observed by DNMR.

(17) (a) Hine, J.; Skoglund, M. J. *J. Org. Chem.* **1982**, *47*, 4766. (b) Nadler, E. B.; Rappoport, Z. *J. Am. Chem. Soc.* **1987**, *105*, 2112.

(18) (a) Fischer, P. In *The Chemistry of Functional Groups. Supplement E. The Chemistry of Ethers, Crown Ethers, Hydroxyl Groups and Their Sulphur Analogs*; Patai, S., Ed.; Wiley: Chichester, 1980; Chapter 17, p 761. (b) Maciel, G. E. *J. Phys. Chem.* **1965**, 1947. (c) Chandrasekaran, S. In *^{17}O NMR Spectroscopy in Organic Chemistry*; Boykin, D. W., Ed.; CRC Press: Boca Raton, FL, 1991; Chapter 7, p 141.

(19) Jorgensen, W. L.; Severance, D. *J. Am. Chem. Soc.* **1990**, *112*, 4786.

ping geminal ring and vicinal rings. The lowest two-ring flip barrier is for **3c** when the nonflipping ring is trans to the OPr-*i*, suggesting that interactions involving OPr-*i* overwhelm the flipping-ring/nonflipping-ring interactions in the transition state. The effect of OPr-*i* is mostly steric, since its conjugation with a planar β- or β'-ring is approximately the same, but such conjugation (cf. **18c**) may increase the barrier for the β,β'-two-ring flip.

The conformation of the OPr-*i* group strongly affects the barrier and it is probably different in the four transition states as could be deduced from the energy vs θ_1 profiles of Figure 5 and from Table 4. Such a conformation effect will be important for other vinylic groups X, e.g. OAc, and together with different degrees of conjugation it contributes to the higher three-ring flip barrier of **1b** compared with **1c**.

Conclusions. Labeling the rings of trimesitylvinyl isopropyl ether by a *m*-MeO group enabled measurement of four barriers for helicity reversal by correlated rotation of the three aryl rings. The order α,β,β'-three-ring flip < α,β'-two-ring flip < α,β-two-ring flip < β,β'-two-ring flip reflects contributions from *o*-Me/*o*-Me interactions, steric effects of the nonflipping rings with vicinal and geminal groups, conjugation effects, and different OPr-*i* group conformation in the different transition states.

MM calculations of the ground-state structure reasonably agree with the X-ray structure of **1c** and correctly predict the qualitative order of the energies of diastereomeric pairs for each of the isomeric ethers **2c**–**4c**. The calculated transition states energies are appreciably lower than the experimental values, probably due to distortion of the rings from planarity. Imposing planarity and in some cases *o*-Me constraints improve in most cases the agreement between the calculated and observed barriers for these systems and for tri- and tetramesitylethylene. The calculations show that three of the transition states for helicity reversal can be achiral or close to it. For the β,β'-two-ring flip, the chiral transition state when the OPr-*i* group is in a clinal staggered conformation with $\theta_1 = 79°$ and $\theta_2 = 57°$ is of lower energy.

Experimental Section

General Methods. Melting points were determined with a Thomas Hoover apparatus and are uncorrected. IR spectra were taken with a Perkin-Elmer Model 157G spectrometer. EI mass spectra were recorded with a MAT-311 instrument at 70 eV. ^{1}H NMR spectra were recorded on a Bruker WP200SV and AMX 400 pulsed FT spectrometers operating at 200.133 and 400.266 MHz, and ^{13}C NMR spectra were recorded on the same spectrometers operating at 50.30 and 100.61 MHz, respectively, with TMS as a reference.

Solvents and Materials. THF was stored over benzophenone ketyl, and ether was stored over $LiAlH_4$. Both were distilled under argon immediately before use. Other solvents were commercial and were used without further purification.

(E)- and (Z)-2-(*m*-Methoxymesityl)-1,2-dimesitylethanol (3a and 4a). (a) 1-Methoxy-2,4,6-trimethylbenzene. To a solution of 2,4,6-trimethylphenol (18.3 g, 135 mmol) in 10% aqueous NaOH (92 mL) was added dimethyl sulfate (20 mL, 211 mmol), and the mixture was stirred overnight. The phases were separated, the former was then extracted with ether (150 mL), and the combined organic phases were washed with 5% aqueous NaOH solution (150 mL) and thrice with water (3 × 200 mL), dried ($MgSO_4$), and evaporated. The remaining liquid (18.2 g, 90%) was distilled in vacuo and the fractions boiling at 36–44 °C at 0.5 torr gave pure 1-methoxy-2,4,6-trimethylbenzene (14.9 g, 74%).

(b) (*m*-Methoxymesityl)mesitylacetic acid (5). A solution of 1-methoxy-2,4,6-trimethylbenzene (4.2 g, 28 mmol) and mesitylglycolic acid[20] (3.5 g, 18 mmol) in AcOH (26 mL) containing H_2SO_4 (17 mL) was kept at room temperature for 9 days. The mixture was poured into water/ice (250 mL) and the white precipitate was collected and washed with water (300 mL). ^{1}H NMR showed the presence of a substantial amount of 1-methoxy-2,4,6-trimethylbenzene. The mixture was dissolved in 10% aqueous NaOH (150 mL) and extracted with ether (100 mL), and the aqueous phase was filtered and acidified up to pH = 4 by a dropwise addition of concd HCl. The white emulsion formed was extracted with ether (200 mL), dried ($MgSO_4$), and evaporated, leaving a white solid: mp 132–3 °C (3.1 g, 53% after drying in vacuo); IR (Nujol) ν_{max} 1705 (C=O, s), 1090 (which is absent in $Mes_2CHCOOH$) cm^{-1}; ^{1}H NMR ($CDCl_3$) δ 2.05 (3H, s, Me), 2.09 (9H, s, 3Me), 2.23 (6H, s, 2Me), 3.62 (3H, s, OMe), 5.36 (1H, s, CH), 6.79 (3H, s, ArH); MS (EI, 70 eV, 120 °C) *m/z* (relative abundance, assignment) 326 (50, M), 281 (B, (MeOMes)CHMes), 206 (51, (MeOMes)CHCOOH), 176 (52, MesCHCOO), 149 (51, MeOMes), 133 (48, $C_6H_2Me_4$?), 119 (31, Mes), 91 (38, C_7H_7), 77 (22, Ph). Anal. Calcd for $C_{21}H_{26}O_3$: C, 77.27; H, 8.03. Found: C, 76.96; H, 7.84%.

(c) (*m*-Methoxymesityl)mesityl ketene (6). To a solution of acid **5** (2 g, 6.1 mmol) in toluene (30 mL) containing pyridine (1 drop) was added thionyl chloride (0.56 mL, 7.7 mmol) and the solution was refluxed for 2 h. The crude product which according to ^{1}H NMR is mainly the ketene (1.8 g, 95%) was recrystallized from petroleum ether 60–80 °C, giving 0.90 g (48%) of the solid yellowish ketene: mp 90–93 °C; IR (Nujol) 2105 (C=C=O, s) cm^{-1}; ^{1}H NMR ($CDCl_3$) δ 2.05 (3H, s, Me), 2.10, 2.11 (9H, 2s, Me), 2.25, 2.26 (6H, 2s, Me), 3.65 (3H, s, MeO), 6.87 (3H, s, ArH). Anal. Calcd for $C_{21}H_{24}O_2$: C, 81.78; H, 7.84. Found: C, 81.51; H, 7.72%.

(d) (E)- and (Z)-2-(*m*-Methoxymesityl)-1,2-dimesitylethanol (3a and 4a). To mesityl magnesium bromide (prepared from bromomesitylene (0.86 g, 4.3 mmol) and Mg turnings (0.11 g, 4.5 mmol) in THF (12 mL) was added during 20 min **6** (0.9 g, 2.9 mmol) in dry THF (15 mL), and the mixture was refluxed for 2.5 h, after which TLC showed that the reaction was completed. The solution was poured into a saturated aqueous NH_4Cl solution (100 mL) and extracted thrice with ether (3 × 50 mL). The ethereal solution was dried ($MgSO_4$), leaving a yellow oil of a 1:1 mixture of the *E* and *Z* isomers (by integration of the MeO signals). Crystallization from petroleum ether 40–60 °C or MeOH gave a mixture of 2-(*m*-methoxymesityl)-1,2-dimesitylethenol (**3a** and **4a**), mp 156–8 °C (0.61 g, 49%). On slow crystallization from petroleum ether or MeOH only the *E* isomer (by X-ray diffraction) had been crystallized. Anal. Calcd for $C_{30}H_{36}O_2$: C, 84.07; H, 8.47%. Found: C, 83.98; H, 8.49.

When the enol is dissolved in a solvent, a $Z \rightleftharpoons E$ isomerization to the equilibrium mixture is observed both by TLC and NMR. The *E*/*Z* equilibrium ratio in $CDCl_3$ at 295 K is 1.11 (based on the MeO signals). The ratio of the helicity diastereomers is 2.23 for the *E* and 1.4 for the *Z*-isomer at 295 K.

In the ^{1}H NMR of the equilibrium mixture in $C_6D_5NO_2$ at 200 MHz at 293 K are observed 22 Me signals (theoretical maximum 36), 4 MeO signals (4), 3 OH signals (4), and 10 ArH signals (maximum expected 20). In $CDCl_3$ containing one drop of DMSO-d_6 all 4 OH signals are observed. The relatively rapid isomerization in solution or on silica column (where it is qualitatively faster) prevents separation of the isomers.

(*E*)- and (*Z*)-2-(*m*-Methoxymesityl)-1,2-dimesitylvinyl Isopropyl Ethers (3c and 4c). To a solution of (*E*)-2-(*m*-methoxymesityl)-1,2-dimesitylethenol (**3a**) (257 mg, 0.6 mmol) in *i*-PrBr (20 mL) were added a solution of 50% aqueous NaOH (10 mL) and solid $PhCH_2N^+Et_3Br^-$ (TEBA) (70 mg, 0.31 mmol), and the mixture was refluxed with stirring overnight. The aqueous phase was extracted with ether (30 mL), and the organic phase was washed with water (3 × 10 mL), dried ($MgSO_4$), and evaporated. The remaining oil (288 mg, 88%) is a 1:1 mixture of the isopropyl ethers according to ^{1}H NMR.

(20) Fuson, R. C.; Emerson, W. S.; Gray, H. W. *J. Am. Chem. Soc.* **1939**, *61*, 480.

The oil was chromatographed on silica (230–400 mesh) using chloroform as the eluent. The *E*-isomer (89 mg) was eluted before the *Z*-isomer (83 mg). Crystallization of the first fraction from MeOH gave pure (*E*)-2-(*m*-methoxymesityl)-1,2-dimesitylvinyl isopropyl ether (**3c**) as a white solid (76 mg, 27%), mp 160 °C. Crystallization of the second fraction from MeOH gave the pure *Z*-ether (66 mg, 23%), mp 157–158 °C.

3c: ^{1}H NMR ($CDCl_3$, 295 K) shows the presence of two diastereomers A and B in 3:1 A/B ratio. [Relative integration is given separately for each isomer.] **A**: δ 0.95, 1.13 (2 × 3H, 2d, J = 6.2 Hz, $CHMe_2$), 1.81, 1.83, 1.86, 1.88, 2.10, 2.19, 2.25, 2.37, 2.59 (27H, 9s, Me), 3.26 (3H, s, OMe), 3.88 (1H, hep, $CHMe_2$), 6.57, 6.58, 6.70, 6.84, 6.93 (5H, 5s, ArH). **B**: δ (signals in italic overlap those of the main isomer) *0.93*, *1.11* (2 × 3H, 2d, J = 6.2 Hz, $CHMe_2$), 1.73, 1.86, 2.11, 2.22, *2.25*, 2.34 *2.37*, 2.61 (27H, 8s, Me), 3.50 (3H, s, MeO), ca. *3.85* (1H, m, *CHMe*$_2$), 6.49, 6.59, 6.68, 6.82 (4 × 1H, 4s, ArH), *6.93* (1H, s, ArH); ^{13}C NMR ($CDCl_3$) δ (A isomer only) 15.52, 17.30, 20.43, 20.73, 20.85, 21.16, 21.20, 21.73, 23.27, 24.65 (Me, CMe_2), 58.88, 69.34 (*o*-CH_3, O*C*H), 117.95, 127.25, 127.86, 128.37, 128.50, 129.41, 131.14, 132.08, 133.73, 134.68, 135.68, 137.03, 137.26, 137.51, 137.93, 137.96, 138.54, 151.84, 155.07 (ArC + C=C); mass spectrum (70 eV, 90 °C) *m/z* (relative abundance, assignment) 470 (61, M), 468 (6, M − H_2), 456 (10, M − CH_2), 428 (100, M − Me_2C), 413 (16, M − Me_2C − Me), 412 (16, M − Me_2CH − Me), 397 (7, M − Me_2CH − 2Me), 249 (16). Anal. Calcd for $C_{33}H_{42}O_2$: C, 84.21; H, 8.99. Found: C, 83.93; H, 8.86%.

4c: ^{1}H NMR ($CDCl_3$) shows two diastereomers in a 1:4 (**A**: **B**) ratio. **A**: δ 0.94, 1.10 (2 × 3H, 2d, J = 6.2 Hz, $CHMe_2$), 1.73, 1.84, 1.86, 1.88, 2.11, 2.23, 2.25, 2.34, 2.55 (27H, 9s, Me), 3.76 (3H, s, OMe), 3.84 (1H, hep, *C*H), 6.50, 6.57, 6.60, 6.73, 6.83 (5H, 5s, ArH). **B**: δ 3.54 (3H, s, OMe); most of other signals partially overlap those for isomer **A**; mass spectrum (70 eV, 90 °C) *m/z* (relative abundance, assignment); 470 (96, M), 468 (4, M − H_2), 428 (100, M − Me_2C), 413 (21, M − Me_2C − Me), 412 (26, M − Me_2CH − Me), 398 (7, M − Me_2C − 2Me), 266 (15), 249 (5). Anal. Calcd for $C_{33}H_{42}O_2$: C, 84.21; H, 8.99. Found: C, 84.45; H, 8.87%.

1-(*m*-Methoxymesityl)-2,2-dimesitylvinyl Isopropyl Ether (2c). 1-(*m*-Methoxymesityl)-2,2-dimesitylethenol (**2a**) was prepared as described previously[4a] from 1-bromo-3-methoxy-2,4,6-trimethylbenzene (966 mg, 4.2 mmol), Mg turnings (103 mg, 4.2 mmol), and dimesitylketene (1.65 g, 6 mmol). The crude oil obtained after workup was dissolved, without further purification, in *i*-PrBr (100 mL), to which $PhCH_2N^+Et_3Br^-$ (0.5 g, 5 mmol) and 50% aqueous NaOH (70 mL) was added and the mixture was refluxed overnight. After extraction with ether (3 × 50 mL), the organic phase was washed with water (3 × 50 mL), dried ($MgSO_4$), and evaporated, leaving a yellow oil (1.68 g). Crystallization (MeOH) gave colorless crystals of 1-(*m*-methoxymesityl)-2,2-dimesitylvinyl isopropyl ether (**2c**) (1.38 g, 70% based on the 1-bromo-3-methoxy-2,4,6-trimethylbenzene): mp 138–9 °C; ^{1}H NMR ($CDCl_3$, 295 K) δ (the ether is ca. a 1:1 mixture of diastereomeric forms A and B) 0.93 (3H, d, J = 6.2 Hz, $CHMe_2$-B), 0.95 (3H, d, J = 6.2 Hz, $CHMe_2$-B), 1.11 (3H, d, J = 6.2 Hz, $CHMe_2$-A), 1.14 (3H, d, J = 6.2 Hz, $CHMe_2$-A), 1.79 (×2), 1.84, 1.88, 1.90 (×2), 1.91 (×2), 2.08, 2.12, 2.215, 2.22, 2.26 (×2), 2.31, 2.32, 2.595, 2.61 (18H, 14s, Me-A + B), 3.31, (2.8H, s, MeO-B), 3.73 (2.8H, s, MeO-A), 3.82 (1H br m, $CHMe_2$), 3.92 (1H, hep, $CHMe_2$), 6.48, 6.51 (2 × 1H, 2s, ArH), 6.57 (2H, s, ArH), 6.64 (1H, s, ArH), 6.71 (2H, br s, ArH), 6.84, 6.93, 6.94 (3 × 1H, 3s, ArH); mass spectrum (70 eV, 70 °C) *m/z* (relative abundance, assignment) 470 (66, M), 428 (100, M − Me_2C), 413 (16, M − Me_2C − Me), 412 (33, M − Me_2CH − Me), 398 (4, M − Me_2C − 2Me), 296 (14), 236 (12). Anal. Calcd for $C_{33}H_{42}O_2$: C, 84.21; H, 8.99. Found: C, 84.48; H, 9.29%.

Crystallographic Parameters. 3a: $C_{30}H_{36}O_2$: M = 428.6; space group $P2_12_12_1$; a = 14.012(2) Å; b = 15.778(2) Å; c = 11.551(3) Å; V = 25537(8) Å^3; Z = 4; ϱ_{calcd} = 1.12 g cm^{-3}; μ(Cu Kα) = 4.53 cm^{-1}; no. of unique reflections = 2078; no. of reflections with $I \geq 2\sigma(I)$ = 1876; R = 0.075; R_w = 0.115; $W^{-1} = \sigma_F^2 + 0.001124F^2$.

3c: $C_{33}H_{42}O_2$. M = 470.7; space group $I2/a$; a = 41.73(1) Å; b = 8.468(2) Å; c = 16.090(3) Å; β = 90.91(1)°; V = 5685(3) Å^3; Z = 8; ϱ_{calcd} = 1.10 g cm^{-3}; μ(Mo Kα) = 0.62 cm^{-1}; no. of unique reflections = 3986; no. of reflections with $I \geq 2\sigma(I)$ = 2316; R = 0.072; R_w = 0.083.

X-ray Crystal Structure Analysis. Data for **3c** were measured on a PW1100/20 Philips four-circle computer controlled diffractometer and for **3a** on an Enraf-Nonius CAD-4 automatic diffractometer. The method and the calculations[21] (using the SHELXS-86 analysis[21a]) were previously described.[17b]

Acknowledgment. We are grateful to Dr. Silvio Biali, Prof. Yitzhak Apeloig, and Mr. Moshe Nakash for discussions and to Dr. Shmuel Cohen for the X-ray crystallography. The work was partially supported by the Commission for Basic Research, Israel Academy for Sciences and Humanities, and by a grant by the Ben-Gurion Fund from the Israel Ministry of Science to E.R., to which we are indebted.

(21) (a) Sheldrick, G. M. *Crystallographic Computing 3*; Oxford University Press: Oxford, UK, 1985; pp 175–189. (b) All crystallographic computing was done on a CYBER 855 computer at the Hebrew University of Jerusalem.